Passive Control of Jets with Indeterminate Origins

R. W. Wlezien* and V. Kibens†
McDonnell Douglas Corporation, St. Louis, Missouri

Control of the development of initially circular jets using inclined and stepped exit geometries is described. The nozzle shape is shown to produce significant modification of the mean flowfield in cases where the shear layer is thick relative to the nozzle diameter. Local enhancement and suppression of shear-layer growth are observed for certain conditions. Augmentation of shear-layer growth results from self-excitation; flow perturbations induced by the shear-layer sectors which develop over the longest run length excite the instabilities in other portions of the layer. The dominant shear-layer scales are determined by the local distance from the nozzle lip, and control is achieved by modifying the azimuthal distribution of energy in the shear-layer instability modes.

Introduction

VARIATION of nozzle geometry constitutes a passive means for controlling the characteristics of an evolving jet. In this sense, control is defined as the capacity to modify the development of the flowfield by directing energy into selected turbulence scales. The augmentation of large scales promotes mixing and entrainment; conversely, interference with their formation can reduce jet noise.[1] Asymmetric jet development can also be used to modify jet noise directivity without necessarily reducing the overall acoustic energy radiated from the jet.

Asymmetric nozzle configurations known to modify shear-layer turbulence characteristics include elliptic[2,3] and rectangular[4] nozzles. Initial spreading enhancement has been observed along the minor axis of elliptic jets, with the direction of preferential growth switching between the minor and major axes with increasing axial distance. Ho and Gutmark[5] attribute the growth differential to mutual induction among the shear-layer vortices, leading to distortion and increased three-dimensionality. In jets with shear layers that do not begin at a single axial position, such as the two-dimensional lip jet[6] in which the upper shear layer is formed before the lower, the velocity perturbations induced by one shear layer can excite the other. Breidenthal[7] investigated the influence of a splitter plate with a spanwise-stepped trailing edge on the development of a single shear layer and concluded that the initial perturbation is soon attenuated.

The geometries considered in the present investigation are designated as indeterminant-origin (I.O.) nozzles because the axial position of the lip varies around the circumference of the nozzle. For axisymmetric jets, the mean velocity profile and the shear-layer momentum thickness are azimuthally invariant. The instability characteristics at any axial location depend on the distance from the nozzle lip and can similarly be expected to be independent of azimuth. Although the most unstable frequencies and dominant shear-layer scales are functions of x/D only, the instability wave system is not necessarily phase-synchronized around the circumference of the jet. For the asymmetric I.O. nozzles, the axial location of the nozzle lip is not constant, and the instability characteristics at a given x/D can therefore be expected to vary with azimuth.

In this paper, the characteristics of jets from inclined and stepped I.O. nozzles are explored. Flow visualization is used to investigate the initial development of the shear-layer modes. Mean-flow measurements illustrate the overall modification of the jet flowfield and jet mixing characteristics. Detailed spectral and modal maps clarify the development of shear-layer instabilities, the self-forcing mechanism, and local mixing augmentation.

Experimental Apparatus and Approach

The two basic I.O. nozzle geometries used in the present investigation, inclined and stepped nozzles, are shown in Fig. 1. The axisymmetric reference nozzle is designated configuration A. The nozzles consist of constant-diameter extensions added to the exit of a contraction section. The mean origin is defined as the average axial location of the nozzle lip. Nozzles with incline and step lengths of $D/2$, D, and $2D$ were investigated. The jet coordinate system is also shown in Fig. 1, with the azimuth angle ψ defined relative to the lowest point of the nozzle.

Nozzles with diameters of 25.4 and 63.5 mm were fabricated and are designated as series 1 and 2, respectively. For a given jet-exit velocity, the series 1 nozzle has a thicker shear layer relative to the nozzle diameter. The nozzle length, defined as the distance from the exit plane of the contraction to the mean origin, is $2.5D$.

The nozzles were mounted to the contraction using an indexing adapter, which allowed them to be rotated to arbitrary azimuthal positions. The jet facility consists of a low-angle conical diffuser followed by a settling chamber with a honeycomb and screens and a 23:1 area ratio bicubic contraction. An electronically controlled blower and a muffler provides a stable, quiet flow source. The flow quality was carefully evaluated, and measures were taken to minimize disturbances at the blower blade-passing and flow-system resonance frequencies. For example, the volume of the system between the blower and the diffuser was increased, effectively damping low-frequency unsteadiness. The intensity of turbulent velocity fluctuations at the jet-exit centerline was reduced to 0.03% at an exit velocity of 30 m/s. By using two-sensor cross correlations, irrotational low-frequency surging was determined to be no more than 0.15% of the jet mean velocity.

The nozzle installation is shown in Fig. 2. An injection plenum was installed immediately upstream of the nozzle to permit flow visualization. Tracer materials were selectively bled into the boundary layer through a circular slit immediately upstream of the nozzle. The channel between the plenum and the injection slit was aligned nearly parallel to the flow direction to minimize the disturbance caused by the

Presented as Paper 84-2299 at the AIAA/NASA Ninth Aeroacoustics Conference, Williamsburg, VA, Oct. 15-17, 1984; received Oct. 30, 1984; revision received Oct. 25, 1985.

*Scientist, McDonnell Douglas Research Laboratories. Senior Member AIAA.

†Principal Scientist, McDonnell Douglas Research Laboratories. Associate Fellow AIAA.

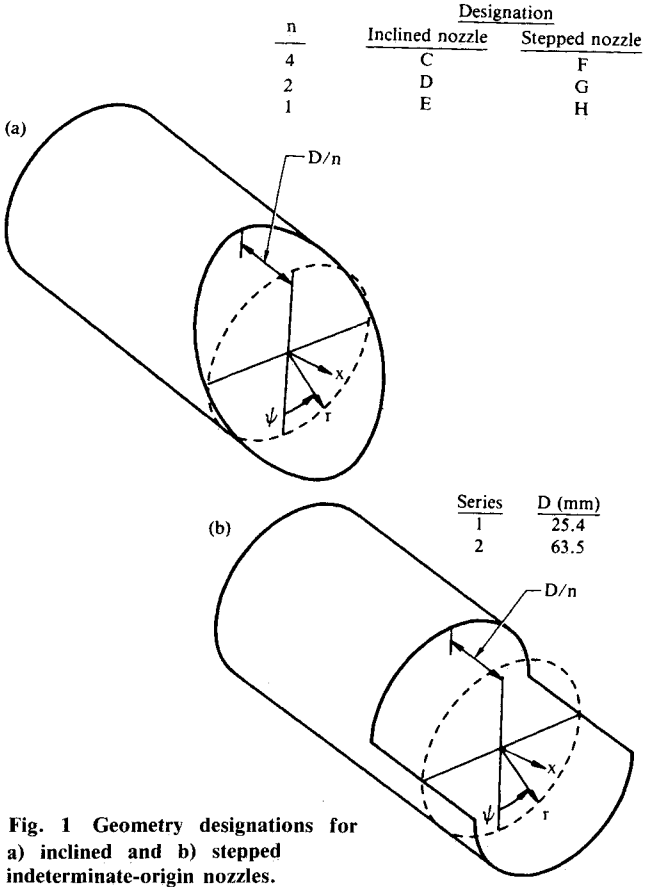

Fig. 1 Geometry designations for a) inclined and b) stepped indeterminate-origin nozzles.

injected flow. Four tubes located around the periphery of the plenum (see Fig. 2) supplied the tracer material. At relatively low jet velocities (<10 m/s) a kerosene aerosol was injected into the flow. Because forward scattering is the most efficient means of illumination, the jet was backlit and photographed against a black background. At greater jet velocities, the smoke was replaced by helium. The density gradients so generated were made visible using a schlieren system with two 400-mm-diam mirrors and a 20-ns-duration spark-gap light source. The schlieren knife edge was aligned normal to the jet axis to provide maximum contrast among the shear-layer vortices.

The flow system was monitored and controlled in real time by a DEC PDP 11/70 data acquisition system. Concurrent routines were used to control the facility, position a three-degree-of-freedom probe traversing system, and acquire data from the experiment. At regular intervals the computer measured the total pressure and temperature in the flow system, as well as laboratory ambient conditions. The jet velocity was automatically maintained within 0.02 m/s of the specified value by a control voltage supplied to the blower motor. The traversing system was driven by stepper motors which positioned a hot-wire sensor with an accuracy of 0.01 mm within a volume of $1\times0.5\times0.5$ m in the x, y, and z directions, respectively.

Hot-wire measurements of the instantaneous axial velocity component were obtained using a Thermo Systems Model 1050 anemometer. Custom sensors were constructed using jewelers' broaches as supports to minimize flow interference. The sensors were recalibrated daily in the jet-exit-plane centerline flow using an automated routine to cycle through 30 calibration velocities. Coefficients were computed for an analog polynomial linearizer that was used for the spectral and modal measurements. For mean velocity and turbulence intensity measurements, the anemometer voltage was directly digitized and linearized using a fourth-order polynomial.

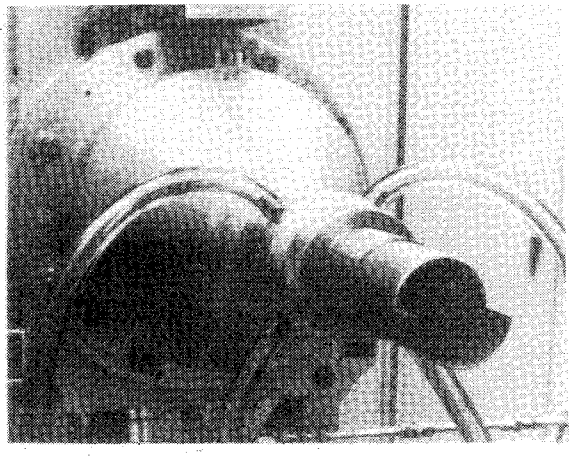

Fig. 2 Test configuration for stepped nozzle.

Detailed mean velocity and turbulence intensity profiles were obtained using a spatial-temporal averaging technique. This method permitted the computation of statistics such as momentum thickness without requiring prohibitively long data acquisition periods. Standard, temporally averaged mean measurements require sufficient averaging time for the statistics to be valid, typically 30 s or more. Detailed profiles of 50-100 points are needed to obtain good estimates of the shear-layer momentum thickness; data acquisition time on the order of 1 h may be required to obtain a single profile. The approach developed here substitutes spatial averaging for long temporal averages.

Data of 0.5 to 1.0 s were acquired and averaged at each sensor position, with a radial increment of $0.01D$ between positions. A full profile of data obtained in this manner required 5 min of acquisition time, which represents a significant decrease over the time-averaged profiles. A sequence of spatial low-pass filters was then applied to the profile to smooth the spatial variation resulting from the short averaging time. The sequence of filters had decreasing spatial cutoff frequencies, so that each successive filter produced a smoother mean profile. Evaluation of the shear-layer momentum thickness provided an objective way to determine the proper degree of smoothing. The smoothing was increased until the computed momentum thickness increased by 2%; the preceding filter was chosen as optimal. As the axial distance from the nozzle increased, the velocity gradients decreased; the energy in the spatial spectrum of the profile effectively moved to lower frequencies. The appropriate spatial cutoff frequency therefore decreased with axial distance from the nozzle.

A similar acquisition scheme was used to determine the spatial distribution of longitudinal turbulent energy for the various shear-layer modes. The linearized hot-wire signal was bandpass-filtered by an analog filter set to the range of 0.8 to $1.25f$, where f represents the mode of interest. This signal was digitized, and 1-s mean-square averages were obtained at each location. The radial and axial increments were $0.01D$ and $0.05D$, for the shear-layer instability f_s and subharmonic $f_s/2$ modes, respectively, and $0.02D$ and $0.1D$ for the $f_s/4$ mode. No spatial averaging was needed because 1 s of data was sufficient to stabilize the narrowband statistics.

Flow Visualization

Figure 3 illustrates the range of shear-layer instability characteristics for series 1 inclined nozzles at a jet Reynolds number Re_D of approximately 6000. The instability wave system for nozzle 1C (Fig. 3a) develops similarly to that for the axisymmetric nozzle: the shear-layer vortices are aligned parallel to the nozzle lip. The inclined vortex forms analogously to that in an axisymmetric jet, thus amplitude

and phase might be expected to be independent of azimuth when the axial coordinate is referenced to the local nozzle lip position.

For the intermediate inclined nozzle 1D (Fig. 3b), the lines of constant phase are not parallel to the nozzle exit, but are inclined at approximately the same angle to the jet axis as those in Fig. 3a. The degree to which the vortex sheet has rolled up clearly decreases along the first and second vortex lines from $\psi = 180$ to 0 deg. The flow asymmetry for nozzle 1E (Fig. 3c) is even greater because the shear-layer instability at $\psi = 180$ deg has developed into discrete vortices before the boundary layer has separated at $\psi = 0$ deg. The disparity between the constant-phase and constant-amplitude lines is clearly greatest for this nozzle. The feature invariant among the nozzles is that the portion of the shear layer which separates first at $\psi = 180$ deg becomes nonlinear at approximately $1D$ from the lip. This segment of the shear layer is not influenced by changes of the nozzle geometry and provides the phase reference for the segments of the shear layer that develop farther downstream.

In Fig. 4, a similar sequence is shown for nozzle 2C at $Re_D = 115{,}000$. The shear-layer thickness and the instability wavelength are significantly smaller relative to the nozzle diameter than for the series 1 nozzles at lower Re_D. The instability system for nozzle 2C (Fig. 4a) is clearly parallel to the nozzle exit, as is the system for nozzle 1C. As the nozzle inclination increases (Figs. 4b and 4c), the continuity of the constant-phase lines is lost and the local constant-phase lines become nearly vertical. A comparison of Figs. 4c and 3c shows that only two discrete vortices exist within the inclined section of nozzle 1E, while as many as nine wavelengths exist within nozzle 2E.

There is evidence of self-excitation for nozzles 1E and 2E because the segment of the shear layer at $\psi = 0$ deg becomes unstable closer to the nozzle lip than the segment at $\psi = 180$ deg. The lines of constant amplitude are not parallel to the nozzle lip; the instabilities that develop first provide an excitation source for the portion of the shear layer that develops farther downstream. For the 1E nozzle, which has a comparatively thick shear layer, the instability takes the form of discrete vortex rings. The decrease in shear-layer scale relative to jet diameter for nozzle 2E eliminates the global organization of the shear-layer instabilities around the periphery of the jet. The initial instability occurs at $\psi = 180$ deg and the phase information propagates circumferentially toward $\psi = 0$ deg as the jet develops downstream. The phasing of the entire shear layer is tied to the initial instability, but the rollup is locally coherent over only about 10 deg.

For a fixed nozzle geometry θ/D decreases as velocity (hence, Re_D) is increased. Figure 5 (nozzle 2D) illustrates the transition from continuous vortex lines to locally coherent instabilities with decreasing θ/D. At $Re_D = 77{,}000$ (Fig. 5a), the development of the upper portion of the shear layer (90 deg $< \psi <$ 180 deg) is similar to that observed in Fig. 3b for configuration 1D, although the vortex lines do not remain continuous through the lower quadrants of the jet. For

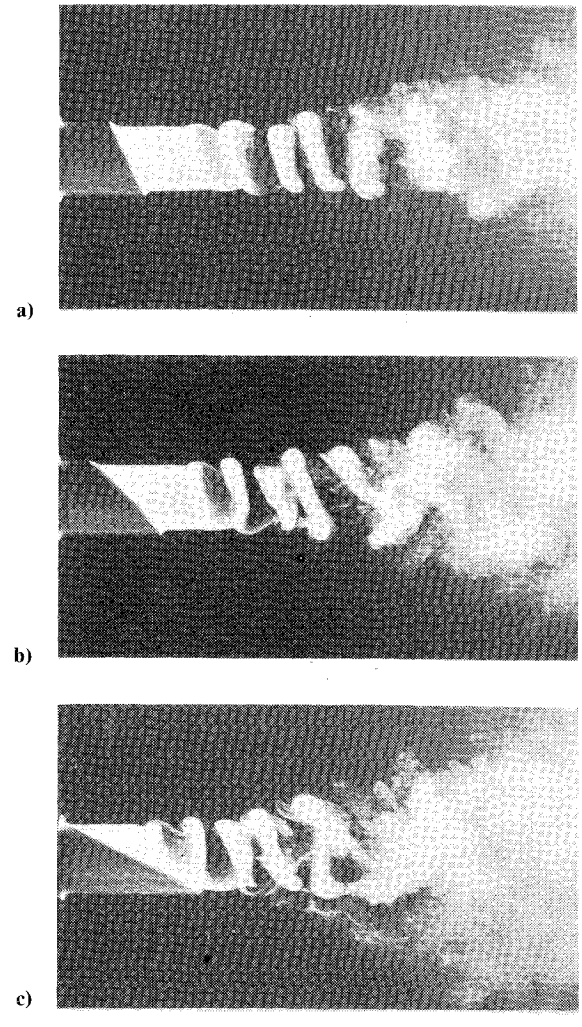

Fig. 3 Development of shear-layer instability for inclined nozzles; $U_0 = 4$ m/s. a) Nozzle 1C, b) nozzle 1D, c) nozzle = 1E.

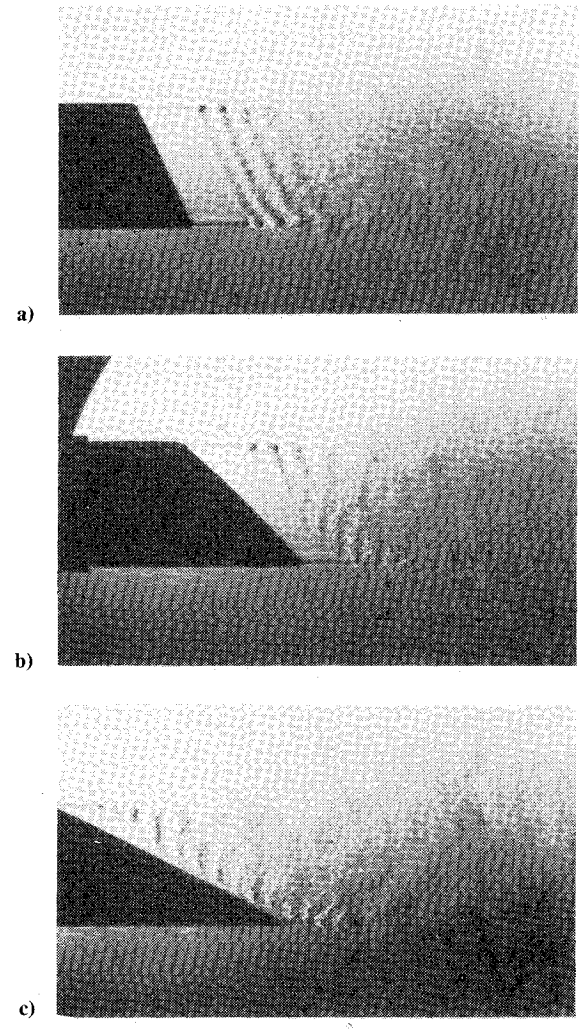

Fig. 4 Development of shear-layer instability for inclined nozzles; $U_0 = 30$ m/s. a) Nozzle 2C, b) nozzle 2D, c) nozzle 2E.

$Re_D = 153{,}000$ (Fig. 5b), the shear-layer instability has shifted to the locally coherent mode, and the instability pattern is similar to that observed for nozzle 2E (Fig. 4c). For inclined nozzles, the characteristics of the shear-layer rollup clearly are dependent not only on nozzle shape, but also on the ratio of the instability wavelength to the nozzle diameter and the ratio of wavelength to incline length.

Instability characteristics of jets from stepped nozzles are shown in Fig. 6. A short step length (nozzle 2F, Fig. 6a) initially produces instability patterns that develop independently for the upper and lower nozzle sections. The upper layer is coherent in amplitude and phase, similar to a jet from an axisymmetric nozzle. The lower shear layer develops similarly, at least in the vicinity of $\psi = 0$ deg; the segments of the vortex lines near $\psi = 90$ deg are deformed, presumably to accommodate the phasing of the upper shear-layer vortices. For a one-diameter step length (nozzle 2G, Fig. 6b), the connection between the upper and lower shear-layer segments is not as obvious because the upper layer has experienced one pairing before the end of the lower nozzle segment. Velocity data discussed in the next section show that the upper and lower halves of this jet develop essentially independently, leading to asymmetry of the mean velocity distributions and shear-layer growth rates.

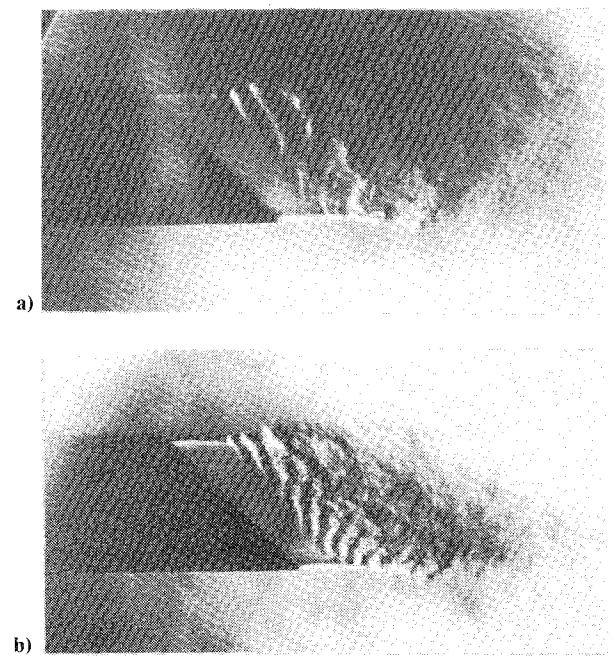

Fig. 5 Variation of instability mode with exit velocity; nozzle 2D. a) $U_0 = 20$ m/s, b) $U_0 = 40$ m/s.

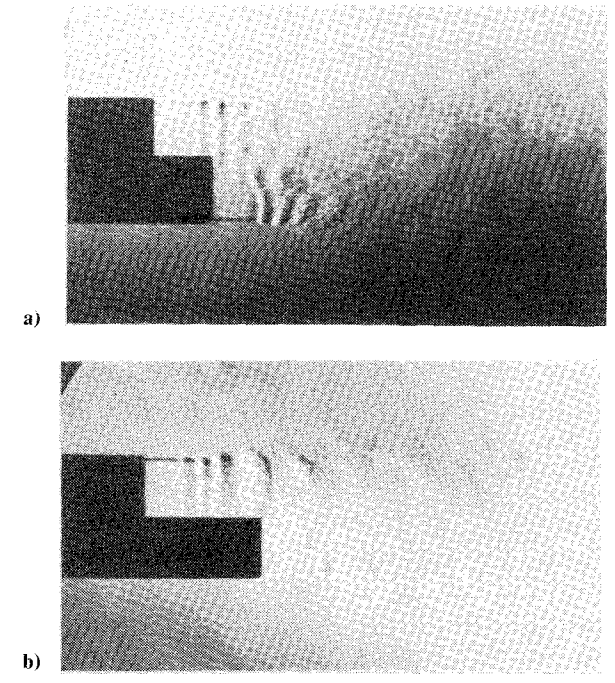

Fig. 6 Development of shear-layer instability for stepped nozzles; a) nozzle 2F, $U_0 = 30$ m/s, and b) nozzle 2G, $U_0 = 20$ m/s.

Mean Velocity Measurements

Mean velocity and turbulence intensity measurements were obtained for the series 1 and 2 nozzles; a representative portion of the data is presented here. The three-dimensional spreading characteristics of the jets were investigated by measuring the axial velocity distribution in planes normal to the jet axis. A custom hot-wire probe was constructed to minimize interference effects. Radial profiles were obtained starting from the jet centerline; the profiles were limited to one side of the jet axis so that the jet did not impinge on the probe body. Profiles were obtained at 15-deg azimuth increments by rotating the nozzle relative to the probe.

The series 1 nozzles proved to be more effective for passive control, probably because their shear layers are thicker with respect to the nozzle diameter. Kibens[8] showed that jets with an initial momentum thickness $\theta/D > 0.005$ have a strong coupling between the initial shear-layer modes and the jet mode that develops at the end of the potential core. The series 1 nozzles fall within this regime for the nominal exit velocity of 30 m/s. For smaller θ/D, such as for the series 2 nozzles, a wavelength selection process that is independent of the initial shear-layer instability determines the scale at the end of the potential core. The flow-visualization results clearly show that the nozzle geometry modifies the

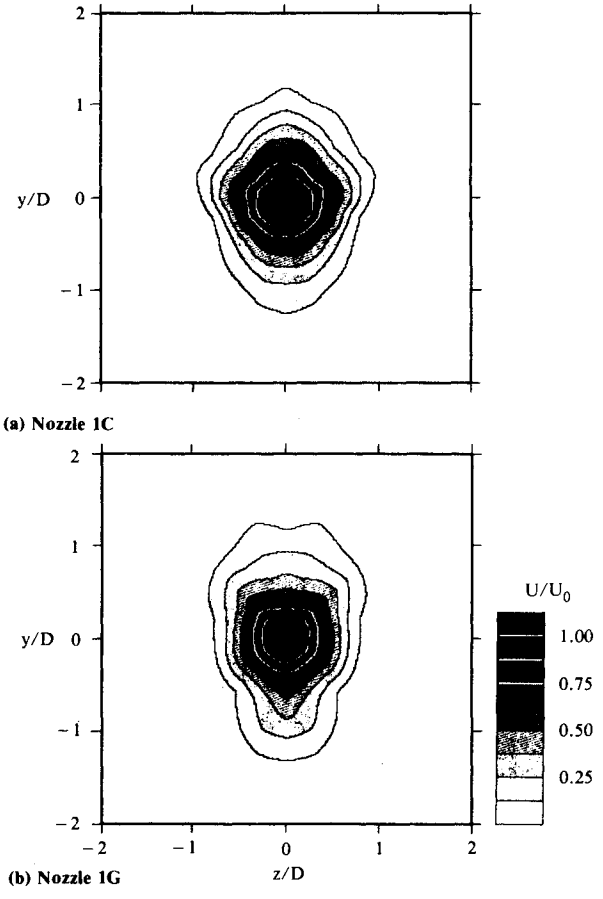

Fig. 7 Mean-velocity distributions in plane normal to jet axis; $x/D = 4$, $U_0 = 32$ m/s.

characteristics of the initial instability, and, therefore, the control scheme is not effective when the initial instability is decoupled from the jet mode.

The series 1 nozzles were operated at a condition that produced a resonance between the flow instabilities and the organ-pipe frequency of the nozzles. The nominal nozzle length of 63.5 mm produces a pipe that could be excited by the subharmonic of the shear-layer instability frequency at an exit velocity of 32 m/s. The resonance condition was chosen because of its similarity to acoustic excitation: the resonance caused the shear-layer pairing locations to be fixed in space and the energy in the instabilities to be concentrated in discrete peaks, thereby facilitating interpretation of velocity spectra. The mean-flow characteristics were qualitatively the same as those for off-resonance conditions.

Figure 7 shows the distribution of mean velocity in a plane normal to the axis of the jet for nozzles 1C and 1G at $x/D=4$. The spreading of these jets exhibited the greatest deviation from the reference configuration at a velocity of 32 m/s. The velocity distributions have significant asymmetry, with spreading enhancement in the vertical plane. The jet from the stepped nozzle has distorted into a nearly elliptic shape, although it is difficult to judge from the velocity distributions alone whether the asymmetry is simply a gross distortion of the mean velocity field, or whether the mixing of the jet is directionally enhanced. To resolve this question, the shear-layer momentum thickness was computed by integrating from the point at which the mean velocity equals 10% of the centerline velocity $U_{c\ell}$ to the 95% point. The normalized momentum thickness

$$\frac{\theta}{D}=2\int_{y_{0.1}}^{y_{0.95}}\frac{U(r)}{U_{c\ell}}\left(1-\frac{U(r)}{U_{c\ell}}\right)\frac{r}{D}\,\frac{\mathrm{d}R}{D} \tag{1}$$

computed for these data is presented in polar form in Fig. 8.

The shear layer is much thicker than that of the reference jet near $\psi=0$ and 180 deg and thinner near $\psi=90$ deg for both the inclined and stepped nozzles, verifying that selective augmentation of mixing has been achieved. It appears that there are two significant effects of passive control, particularly for the 1G stepped nozzle. The first is that shear-layer growth in the $\psi=0$ deg quadrant is greatly enhanced. The lower half of the shear layer spearates one diameter farther downstream than the upper half, yet both shear layers are approximately the same thickness at $x/D=4$. Second, shear-layer development is actually suppressed near $\psi=90$ deg. Because the velocity difference between the jet centerline and the ambient fluid is the same for all azimuths, the lateral shear layers have greater velocity gradients than those of the reference configuration. The flow visualization discussed earlier shows coherent instabilities only at the azimuths for which spreading is enhanced. The initial condition imposed by the stepped exit essentially splits the shear layer into two halves; mixing is concentrated in the middle of each half and suppressed in the transition region between them.

The axial development of the shear-layer momentum thickness and the longitudinal turbulent energy for nozzle 1C is shown in Fig. 9. The normalized longitudinal turbulent energy E_u is defined to be the mean square of the fluctuating velocity $\overline{u^2}$ integrated over the same area as the momentum thickness:

$$E_u=8\int_{y_{0.1}}^{y_{0.95}}\frac{\overline{u^2(r)}}{U_0^2}\,\frac{r}{D}\,\frac{\mathrm{d}r}{D} \tag{2}$$

The growth of the momentum thickness is suppressed for $\psi=90$ deg (triangle), as might be inferred from the previous figure. The shear layer is thicker than that of the reference jet at $\psi=180$ deg (diamond), even when the origin is shifted to compensate for the upper layer originating at $x/D=-0.25$. The segment of the shear layer at $\psi=0$ deg (square) initially is thinner than that of the round jet because of the short development distance from the local lip position. Over the range $1.5<x/D<2.5$, this shear-layer segment experiences extremely rapid growth and becomes the thickest segment for all subsequent axial locations.

A comparison of the E_u curves at $\psi=0$ and 180 deg indicates a rapid increase of the turbulent energy in the lower layer over the same axial range. The lower shear layer is initially the least active, but the turbulence level grows rapidly and surpasses that of the upper layer near $x/D=2$. It is possible to interpret this result in terms of the self-excitation phenomenon observed in the flow-visualization photographs. The upper shear layer develops first and is free to become unstable at a frequency determined by its instability characteristics. The lower layer, on the other hand, grows under the influence of the perturbations induced by the upper

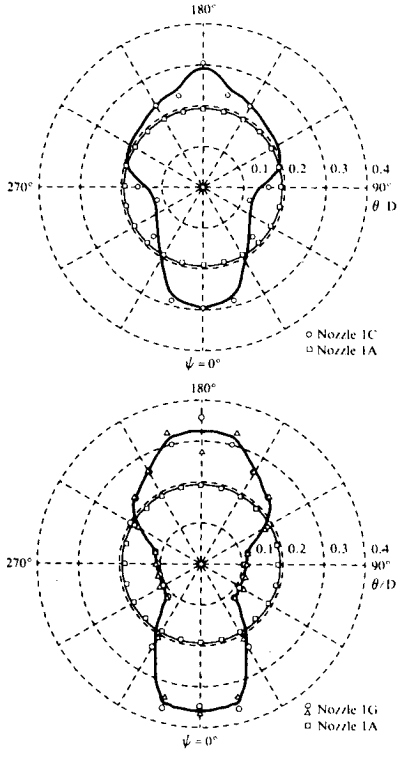

Fig. 8 Azimuthal dependence of momentum thickness, θ/D; $x/D=4$, $U_0=32$ m/s.

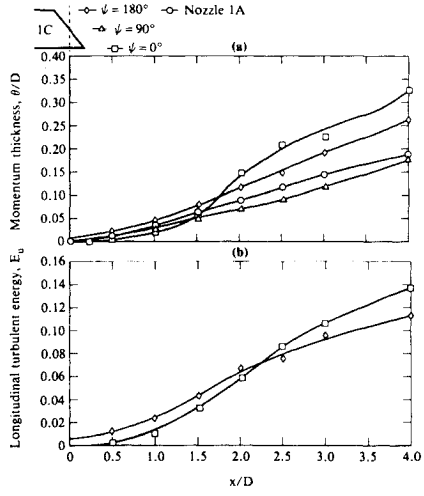

Fig. 9 Azimuthal variation of axial development of momentum thickness and longitudinal turbulent energy for nozzle 1C; $U_0=32$ m/s.

layer. These perturbations amount to forcing of the lower layer by the unsteady induced velocity field generated by the upper shear-layer segment. Detailed unsteady flow measurements in the next section clarify the self-excitation mechanism further.

Development of Shear-Layer Instability Frequencies

Axial development of shear-layer instability frequencies was investigated using a spectral mapping technique. The spectral measurements were limited to a single radius for each axial location because of the time required to obtain valid spectral estimates. The proper choice of sensor position therefore became a prime consideration. Centerline measurements have been used in previous investigations because the potential core filters out all but the strongest irrotational perturbations induced by the shear-layer vortices. However, centerline measurements are difficult to interpret because 1) the velocity perturbations at the centerline are induced by the entire shear layer and, therefore, are not axially selective, and 2) the shear-layer vortices approach the centerline with distance from the nozzle lip, artificially increasing the magnitude of the centerline velocity perturbations. The half-diameter line and center of the shear layer are also undesirable because the small-scale turbulence masks the signatures of the coherent vortices. The inner edge of the shear layer, operationally defined as the line along which the mean velocity is 95% of the jet-exit velocity, was determined to be a location for which the irrotational perturbations induced by the large scales could be measured in an unbiased manner.

Figure 10 shows the axial development of the shear-layer spectra for the axisymmetric nozzle 2A at an exit velocity $U_0 = 40$ m/s. The sensor location was automatically selected under computer control using an iterative scheme to find the $0.95U_0$ line; the position reverted to the jet centerline beyond the end of the potential core. The spectral maps consist of one-twelfth-octave spectra[1] measured at logarithmically spaced axial locations. The progression of shear-layer instabilities to decreasing frequencies is represented by the gray regions of the map. The initial instability and two subsequent pairings are identified by the energy concentrations at $St_D = 8$, 4, and 2. The instability process clearly does not select discrete frequencies beyond the second pairing, and the frequency of the spectral peak decreases in a uniformly continuous manner. The centerline of the jet becomes contaminated with small-scale turbulence beyond $x/D = 7$, with attendant broadening of the spectrum.

Similar maps obtained for a variety of nozzle geometries, azimuth angles, and exit velocities were processed to yield energy-weighted average frequencies at each axial location relative to the local nozzle lip position, x_0. The energy-weighted averages were obtained by computing the center of mass of individual spectra over the range for which the normalized fluctuation level $u'(f)/U_0$ remained above -40 dB. This level corresponds to the boundary of the lightest gray region in Fig. 10 and is an objective way to compare the development of the instability frequency among configurations. The results for a series of runs for inclined and axisymmetric nozzles are shown in Fig. 11a. When the Strouhal numbers are computed in terms of nozzle diameter and plotted as a function of distance from the local nozzle lip, the data collapse to a curve that can be approximated by

$$St_D[(x-x_0)/D] = 1.5 \tag{3}$$

at least for $(x-x_0)/D < 4$.

The significance of this apparently universal curve is that the local Strouhal number is determined solely by the distance from the nozzle lip. The collapse of the data was not limited to those shown in Fig. 11; the data for all nozzle configurations were remarkably consistent, with the exception of the stepped nozzle at $\psi = 90$ deg, an azimuth for

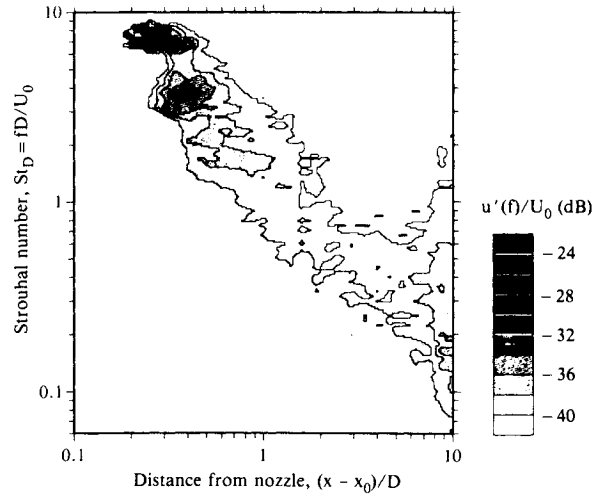

Fig. 10 Axial spectral development along $0.95U_0$ line for nozzle 2A; $U_0 = 40$ m/s.

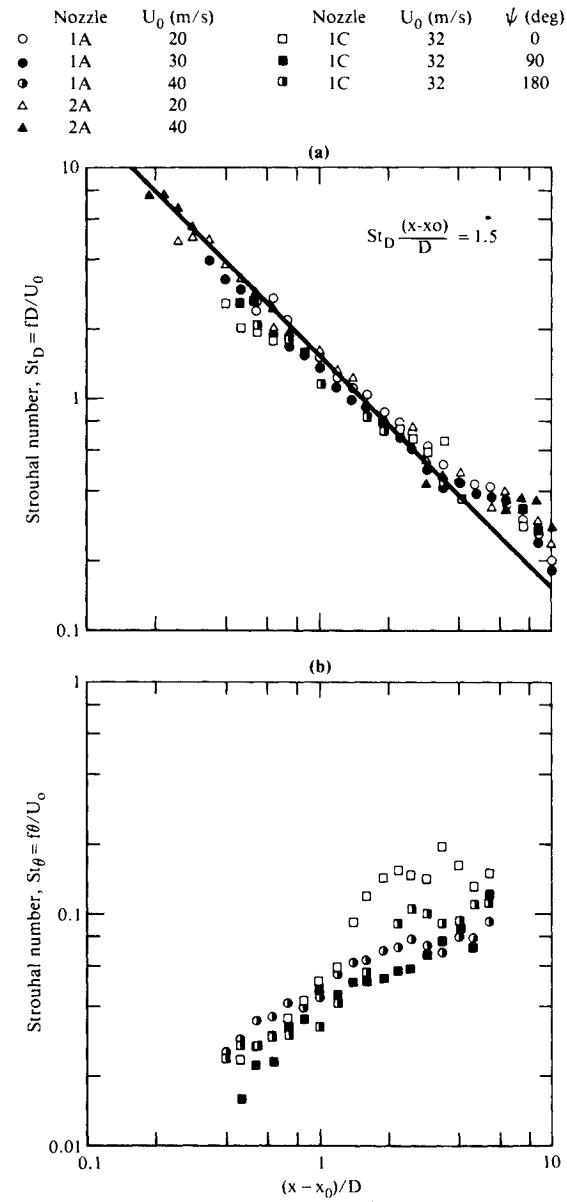

Fig. 11 Variation of mean St_D and St_θ with axial distance from nozzle lip along $0.95U_0$ line.

which the lip position is not well defined. The averages follow the curve even for small distances from the lip, where the turbulent energy is restricted to discrete peaks. One interpretation consistent with these results is that the various scales grow and decay as the local shear layer becomes unstable and stable, respectively, to a particular range of frequencies.

Figure 11b is an attempt to reconcile the local mean frequencies with the local momentum thickness. If linear stability theory were applicable, the most amplified frequency would scale with the local shear-layer thickness, leading to a nearly constant St_θ. St_θ increases by a factor of 5 over the first 10 diameters, which is clearly greater than the most amplified St_θ predicted by Michalke[9] except very near the nozzle exit. There is no reason to expect linear stability theory to predict the shear-layer frequencies after nonlinear interactions occur. However, Fig. 11b demonstrates that the instability process in the shear layer does not scale with the local shear-layer thickness.

On the other hand, the data collapse to the curve of Eq. (3), which is identical to the subharmonic resonance relation given by Laufer,[10]

$$St_D \frac{(x-x_0)}{D}\left(\frac{U_0}{U_c}+\frac{U_0}{a}\right)=N \qquad (4)$$

for a normalized eddy convection velocity $U_c/U_0 \approx 0.5$, a low subsonic exit velocity $U_0/a \approx 0$, and a feedback period of three resonance periods ($N=3$). This model implies that the jet grows by vortex pairing and the pairing positions are determined by feedback to the nozzle lip. The implication is that the local jet scales are governed solely by feedback to the separation point; however, this process is inconsistent with the azimuthal self-excitation observed in the flow visualization.

Regardless of which mechanism is the appropriate model for shear-layer growth, these results clearly illustrate that the instabilities are constrained to follow a succession of frequencies determined by the axial distance from the separation point. Passive control achieved by varying nozzle geometry is therefore limited to changing the total amount of energy in a given scale at a particular streamwise location.

Self-Excitation

The role of self-excitation is explored for the stepped nozzle 1G using the maps of shear-layer mode development shown in Figs. 12 and 13. The intensity of the various shear-layer modes $E_u(f)$ was measured by integrating the square of the bandpass-filtered fluctuating axial velocity across the shear layer at a series of axial locations. The nozzle was rotated in 30-deg increments to provide an azimuthal description of mode development. The axial coordinate was taken relative to the local lip position x_0 to provide a direct comparison of the two shear-layer halves.

Figure 12 shows that the initial shear-layer instability f_s develops as expected from the flow visualization. The instability pattern for the upper half of the nozzle is practically independent of azimuth, with the f_s mode saturating uniformly at $(x-x_0)/D \approx 0.05$. The instability pattern of the lower layer, which actually is farther downstream, is similar to that in the upper layer over the range $-30 \text{ deg} < \psi < 30$ deg when referenced to the local lip position. The implication is that there is no self-excitation for the f_s mode because the instability amplitude is a function only of distance from the nozzle lip. The influence of the step extends over the remainder of the shear layer, although the relatively high intensities at $\psi = 90$ deg are an artifact of filtered broadband turbulent fluctuations, not true f_s instabilities.

The subharmonic $f_s/2$ development is similar to that of the fundamental; the entire upper half of the layer and the segment of the lower layer near $\psi = 0$ deg saturate uniformly at $(x-x_0)/D = 0.6$. However, subharmonic development is different because the modal energy in the lower shear-layer segment is concentrated near $\psi = 0$ deg and pairing is effectively suppressed near $\psi = 90$ deg. The overall distortion of the subharmonic saturation amplitude is consistent with the asymmetry of the mean velocity field.

The two shear-layer halves become more closely coupled with the development of the second subharmonic $f_s/4$, as shown in Fig. 13. There is evidence of self-excitation, because the segment of the shear layer near $\psi = 0$ deg (Fig. 13b) saturates approximately $0.3D$ closer to the lip than the segment at $\psi = 180$ deg (Fig. 13a). If the axial coordinate in Fig. 13 is recast as x/D, the effect is to shift Fig. 13b vertically by D, the length of the step. The azimuthal propagation of the instability thus becomes clear, because the first three contours of constant amplitude are continuous rings inclined with respect to the jet axis. The two halves of the jet do not develop independently, and the $f_s/4$ instability at $\psi = 0$ deg lags that at $\psi = 180$ deg by $0.6D$, as opposed to D if the top and bottom of the jet were independent.

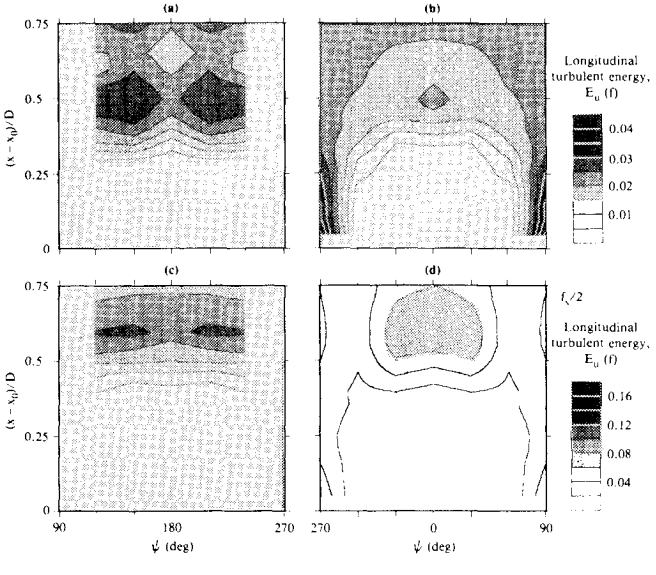

Fig. 12 Development of f_s and $f_s/2$ shear-layer modes as a function of azimuth angle and distance from lip; nozzle 1G, $U_0 = 32$ m/s.

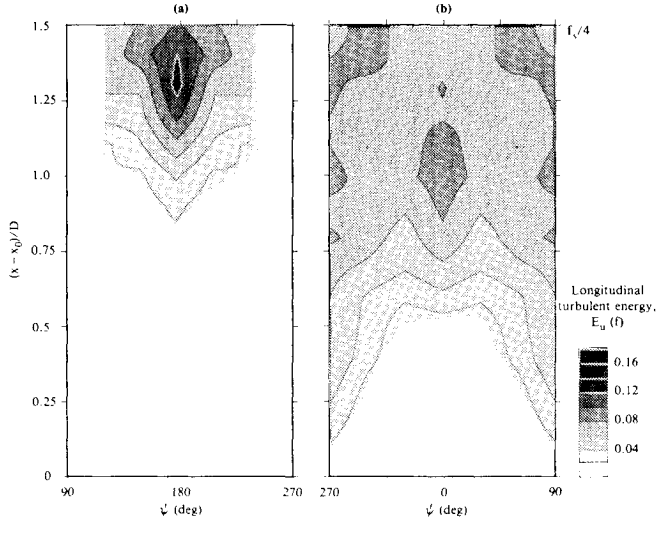

Fig. 13 Development of $f_s/4$ shear-layer mode as a function of azimuth angle and distance from lip; nozzle 1G; $U_0 = 32$ m/s.

Another observation is that the greatest amplitude for the $f_s/4$ mode occurs near $\psi = 0$ and 180 deg. Although the $f_s/4$ mode has saturated well before $x/D = 4$, where strong asymmetry was observed in the mean profiles, it is apparent that asymmetric development of the initial jet instabilities leads to the directional growth of the shear layers farther downstream.

Concluding Remarks

The control of the development of jets from nozzles with stepped and inclined exits has been demonstrated, with attendant distortion of the mean velocity distributions and selective enhancement and suppression of shear-layer growth. The directional nature of the mixing augmentation has potential application to the azimuthal modification of jet noise. The degree of control effected is dependent not only on nozzle geometry, but also on the ratio of the shear-layer instability wavelength to the nozzle scale. Significant flowfield modification is achieved when the shear layer is thick relative to the nozzle diameter. When the scales that develop at the end of the potential core occur at a subharmonic of the initial shear-layer instability frequency, modification of the initial instability through interaction with nozzle geometry directly influences the development of large scales. Conversely, little control is achieved when the large scales form independently of the initial instabilities.

Azimuthally propagating self-excitation appears to be the mechanism by which shear-layer growth is locally augmented. For stepped nozzles, the two halves of the shear layer initially develop independently, with cross-excitation evident in the formation of the second subharmonic frequency. For inclined jets the self-excitation can be achieved by circumferentially propagating instabilities. For both cases, modification of the nozzle geometry does not change the axial hierarchy of instability frequencies. The progression of the instability process to increasingly large scales is universally determined by the distance from the local separation point. The data collapse remarkably well to Laufer's subharmonic resonance model, although azimuthal self-excitation clearly is inconsistent with such a model. The passive control scheme investigated here is restricted to the modification of the azimuthal distribution of energy in the various instability modes, with the hierarchy of modes predetermined by the distance from the separation point.

Acknowledgment

This research was supported under Air Force Office of Scientific Research Contract F49620-83-C-0048.

References

[1]Wlezien, R. W. and Kibens, V., "Shear-Layer Development in an Annular Jet," AIAA Paper 84-0400, 1984.

[2]Gutmark, E. and Ho, C. M., "Near Field Pressure Fluctuations of an Elliptic Jet," AIAA Paper 83-0663, 1983.

[3]Husain, H. S. and Hussain, A.K.M.F., "Controlled Excitation of Elliptic Jets," *The Physics of Fluids*, Vol. 26, Oct. 1983, pp. 2673-2765.

[4]Krothapalli, A., Baganoff, D., and Karamcheti, K., "On the Mixing of a Rectangular Jet," *Journal of Fluid Mechanics*, Vol. 107, 1981, pp. 201-220.

[5]Ho, C. M. and Gutmark, E., "Visualization of the Elliptical Jet," *Bulletin of the American Physical Society*, Vol. 27, Nov. 1982, p. 183.

[6]Ho, C. M. and Hsiao, F. B., "Evolution of Coherent Structures in a Lip Jet," *Structure of Complex Turbulent Shear Flow*, IUTAM Symposium, Marseille, 1982, edited by R. Dumas and L. Fulachier, Springer, Berlin, 1983, pp. 121-136.

[7]Breidenthal, R., "Response of Plane Shear Layers and Wakes to Strong Three-Dimensional Disturbances," *The Physics of Fluids*, Vol. 23, Oct. 1980, pp. 1929-1934.

[8]Kibens, V., "The Limits of Initial Shear-Layer Influence on Jet Development," AIAA Paper 81-1960, 1981.

[9]Michalke, A., "The Instability of a Compressible Circular Jet with Finite Boundary Layer Thickness," (in German), *Zeitschrift für Flugwissenschaften*, Vol. 19, No. 8/9, 1971, pp. 319-338.

[10]Laufer, J., "Instability and Turbulence in Jets," *Transition and Turbulence*, Academic Press, New York, 1981, pp. 63-76.